The building blocks of Northern Hemisphere wintertime stationary waves

Chaim I. Garfinkel*

The Hebrew University of Jerusalem, Institute of Earth Sciences, Edmond J. Safra Campus, Givat Ram, Jerusalem, Israel

Ian White

The Hebrew University of Jerusalem, Institute of Earth Sciences, Edmond J. Safra Campus, Givat Ram, Jerusalem, Israel

Edwin P. Gerber

Courant Institute of Mathematical Sciences, New York University, New York, USA

Martin Jucker

Climate Change Research Center and ARC Centre of Excellence for Climate Extremes, University of New South Wales, Sydney, Australia

Moran Erez

The Hebrew University of Jerusalem, Institute of Earth Sciences, Edmond J. Safra Campus, Givat Ram, Jerusalem, Israel

**Corresponding author address:* Chaim I. Garfinkel, The Hebrew University of Jerusalem, Institute of Earth Sciences, Edmond J. Safra Campus, Givat Ram, Jerusalem, Israel.

E-mail: chaim.garfinkel@mail.huji.ac.il

ABSTRACT

An intermediate complexity moist General Circulation Model is used to investigate the forcing of stationary waves in the Northern Hemisphere boreal winter by land-sea contrast, horizontal heat fluxes in the ocean, and topography. The linearity of the response to these building blocks is investigated. In the Pacific sector, the stationary wave pattern is not simply the linear additive sum of the response to each forcing. In fact, over the northeast Pacific and western North America, the sum of the responses to each forcing is actually opposite to that when all three are imposed simultaneously due to nonlinear interactions among the forcings. The source of the nonlinearity is diagnosed using the zonally anomalous steady-state thermodynamic balance, and it is shown that the background state temperature field set up by each forcing dictates the stationary wave response to the other forcings. As all three forcings considered here strongly impact the temperature field and its zonal gradients, the nonlinearity and nonadditivity in our experiments can only be explained in a diagnostic sense. This nonadditivity extends up to the stratosphere, and also to surface temperature, where the sum of the responses to each forcing differs from the response if all forcings are included simultaneously. Only over western Eurasia is additivity a reasonable (though not perfect) assumption; in this sector land-sea contrast is most important over Europe, while topography is most important over Western Asia.

1. Introduction

Although the solar forcing at the top of the atmosphere is zonally symmetric when averaged over a day or longer, the climate of the Earth is decidedly not zonally symmetric. These zonal asymmetries, or stationary waves, are forced by asymmetries in the lower boundary, such as the land-ocean distribution and orography. The land-ocean distribution directly impacts the distribution of surface temperature and moisture, while mountains directly impact the atmospheric flow (e.g., Held et al. 2002).

Developing a good understanding of the mechanisms controlling the stationary waves is important for many reasons. First, the position and intensity of stationary waves strongly influence the weather and climate of Eurasia and North America. Surface temperature in cities at comparable latitudes differ drastically; for example, London and Calgary are both located at 51°N, while Rome and Chicago are both at 42°N, yet mean winter surface temperatures differ by $\sim$ 10C between these pairs of cities. Second, stationary waves control, in large part, the distribution of storm tracks (e.g., Branstator 1995; Chang et al. 2002; Shaw et al. 2016), which are closely linked to extreme wind and precipitation events (Shaw et al. 2016). Subtle shifts in stationary waves, such as those projected to occur under climate change, can lead to profound impacts on regional climate (Neelin et al. 2013; Simpson et al. 2016). To interpret and have confidence in simulated future changes in the climate of the extratropics, it is important to have a good understanding of the mechanisms for stationary waves in the current climate.

Since pioneering studies by Charney and Eliassen (1949) and Smagorinsky (1953), dozens of modeling studies have examined the forcings most crucial for atmospheric stationary waves, as summarized in the review article by Held et al. (2002). The vast majority of these earlier studies generated stationary waves not by imposing the land-ocean contrast directly, but rather by imposing an asymmetrical distribution of diabatic heating (Held et al. 2002). In boreal wintertime, the imposed diabatic heating turns out to be the most important ingredient for the generation of stationary waves, with eddy fluxes and orography playing smaller roles (Held et al. 2002; Chang 2009), though there is sensitivity to the details of, e.g., the damping, the precise form of the diabatic heating, and the low level winds (Held and Ting 1990).

There is some ambiguity in these results however: diabatic heating is dependent on the flow and thus not independent of orographic forcing (as noted by Held et al. 2002; Chang 2009). That is, the removal of orographic forcing acts to modify surface temperatures (Seager et al. 2002) and the heating distribution, which can then lead to a feedback on the stationary waves. The only way to assess the full impact of the removal of orography involves simulating how the diabatic heating may respond. Similarly, diabatic heating regulates the response to orograpy: Ringler and Cook (1999) found that diabatic heating near Tibet and the Rockies modifies the flow incident on the mountains and alters the stationary wave generated by the mountains. A model which imposes diabatic heating independently from orographic effects cannot capture such a nonlinear effect.

An alternate class of models that has been used to study the generation of stationary waves are models in which diabatic processes are parameterized by the model and can therefore interact with one-another and with topography (e.g., Manabe and Terpstra 1974; Blackmon et al. 1987; Broccoli and Manabe 1992; Kitoh 1997; Inatsu et al. 2002; Wilson et al. 2009; Brayshaw et al. 2009, 2011; Saulière et al. 2012; White et al. 2017). Large-scale orography (in particular the Rockies and Tibetan Plateau) has been found in many of these studies to be the dominant contributor to stationary waves. Land-sea contrast was found to be of secondary importance in forcing stationary waves, by both Inatsu et al. (2002) and Brayshaw et al. (2009), despite the large differences in heat capacity, surface friction, and moisture availability between oceans and continents.

The zonal structure in tropical and extratropical sea surface temperatures (SSTs), however, was found to be critical in shaping the stationary waves, albeit in very different ways. Tropical SST anomalies can influence stationary wave structure by modifying the regions of preferred upwelling in the Walker cell and associated divergent outflow (Inatsu et al. 2002; Brayshaw et al. 2009, among others) and thus act as a localized Rossby wave source. The thermal contrast between relatively warm wintertime oceans and cold wintertime continents in midlatitudes favors winter storm growth in the western part of ocean basins, and this enhancement is particularly strong for a southwest-northeast coastline orientation such as on the eastern coast of North America (Brayshaw et al. 2009, 2011). These eddies can then feed back on the stationary waves (Held et al. 2002; Kaspi and Schneider 2013). However there is some ambiguity when imposing SSTs: Seager et al. (2002) conducted a set of experiments using an atmospheric general circulation model coupled to a mixed layer ocean to assess the impact of orography on the zonal asymmetries in the surface temperature distribution. Their results suggest that, if all mountains are removed, half of the surface temperature contrast between eastern North America and Western Europe (and adjacent oceanic areas) would disappear, owing to a change in surface wind direction and resulting temperature advection.

The models used in these studies generally fall into two categories: first, aquaplanet models in which stationary wave forcings are introduced in an idealized manner, but there is little attempt to reconstruct quantitatively the observed stationary wave field (e.g., Inatsu et al. 2002; Brayshaw et al. 2009, 2011; Saulière et al. 2012), or, second, comprehensive models in which a particular feature is omitted from a complete, "realistic" set of lower boundary conditions (e.g., Kitoh 1997; Broccoli and Manabe 1992; Wilson et al. 2009; White et al. 2017). These comprehensive models, however, tend to be less flexible and tuned such that removing too many relevant forcings leads to unstable behavior. A model that can fully bridge these two categories is currently lacking, though we acknowledge the progress made by Brayshaw et al. (2009, 2011) and Saulière et al. (2012).

While the aforementioned studies have made significant progress towards uncovering the building blocks of stationary waves, there are still several open questions that we address in this study:

1. Can one reconstruct the full magnitude of stationary waves by adding together the individual building blocks?

2. To what extent do the various building blocks of stationary waves interact nonlinearly with each other?

3. How does the degree of nonlinearity change between e.g., the Pacific sector and the Atlantic sector?

4. To the extent that nonlinearities exist, can we provide a diagnostic budget for the emergence of these nonlinearities?

The goal of this work is to attempt to answer these four questions. In order to achieve this goal, we have developed a simplified model that can represent stationary waves as faithfully as comprehensive general circulation models used for climate assessments, yet is still modular enough to allow one to build stationary waves by incrementally adding *all* relevant forcings (namely land-sea contrast, ocean heat fluxes, and orography) to a zonally symmetric aquaplanet, or to remove them incrementally from a model configuration in which all of the forcings are initially present.

After introducing this novel model in Section 2, we document the realism of its stationary waves in Section 3. Section 4a demonstrates that in much of the Northern Hemisphere, the individual building blocks of stationary waves interact non-additively, such that the sum of the responses to each building block does not equal the response when all are imposed simultaneously. The specific interactions among the forcings that lead to this non-additive behavior are documented in

Section 4b, and in Section 4c we use the zonally anomalous steady-state thermodynamic balance to provide an explanation for this non-additivity. Section 5 discusses which specific aspects of heat fluxes in the ocean (e.g., tropical warmpools and warmer extratropical SST near the western boundary) and of land-sea contrast (e.g., land-sea contrast in moisture availability, heat capacity, and surface friction) are most important for forcing stationary waves.

2. A model of an idealized moist atmosphere (MiMA)

We construct an intermediate complexity model that captures the important processes for stationary waves. While the ultimate goal is to understand nature, simpler models are valuable in order to isolate and subsequently synthesize fundamental physical processes, and serve as an important intermediate step between theory and comprehensive climate models. This approach has been espoused by Held (2005) and others as essential to narrowing the gap between the simulation and understanding of climate phenomena. Our goal is not to capture every detail of the observed stationary wave pattern, as even comprehensive general circulation models used in climate assessments do not succeed at this pursuit. Rather our goal is for the stationary waves in the intermediate model to be reasonably accurate, e.g., to fall within the envelope of stationary waves simulated by CMIP5 models.

While it is possible to generate realistic stationary waves with a dry model of the atmosphere through an iterative process (Chang 2009; Wu and Reichler 2018), the physical connection to key forcings such as land-sea contrast in temperature and moisture is lost. Rather, we add three forcing mechanisms of stationary waves to a zonally symmetric moist aquaplanet model: orography, ocean horizontal heat fluxes, and land-sea contrast (i.e., the difference in heat capacity, surface friction, and moisture availability between oceans and continents).

We begin with the model of an idealized moist atmosphere (MiMA) introduced by Jucker and Gerber (2017). This model builds on the aquaplanet model of Frierson et al. (2006), Frierson et al. (2007), and Merlis et al. (2013). It includes moisture (and latent heat release), a mixed-layer ocean, Betts-Miller convection (Betts 1986; Betts and Miller 1986), and a boundary layer scheme based on Monin-Obukhov similarity theory. The Frierson et al. (2006) model uses a grey-radiation scheme and hence cannot resolve the interaction of shortwave radiation with ozone. It therefore lacks a realistic stratosphere. MiMA incorporates the Rapid Radiative Transfer Model (RRTM) radiation scheme (Mlawer et al. 1997; Iacono et al. 2000). The RRTM code is used in both operational forecast systems (e.g., the European Center for Medium-Range Weather Forecasting and the US National Center for Environmental Prediction) and CMIP atmospheric models (e.g., the Max Planck Institute and Laboratory for Dynamical Meteorology models). With this new radiation scheme, we are able to incorporate the radiative impacts of ozone and water vapor into the model. This is in contrast to previous idealized studies of storm tracks and stationary eddies (e.g., Kaspi and Schneider 2013), and allows for the representation of a realistic stratosphere. Gravity waves have been added to the model following Alexander and Dunkerton (1999) and Cohen et al. (2013); this allows for the spontaneous generation of a Quasi-Biennial Oscillation, and the details of the Quasi-Biennial Oscillation in MiMA will be the subject of a future paper. The momentum associated with gravity waves that would leave the upper model domain is deposited in the levels above 0.85hPa in order to conserve momentum.

a. Land-sea contrast

Three different aspects of land-sea contrast are imposed: the difference in mechanical damping of near surface winds between the comparatively rough land surface vs. the smooth ocean, the difference in evaporation between land and ocean, and the difference in heat capacity. The roughness length for both moisture and momentum are varied between ocean and land to approximate land-sea contrasts. The roughness length for momentum over land is set as $5 \cdot 10^3$ larger than its value over ocean (which is $3.21 \cdot 10^{-5}$m), while the roughness length for moisture exchange over land is set $1 \cdot 10^{-12}$ smaller than its value over ocean (which is also $3.21 \cdot 10^{-5}$m). These factors were selected via trial and error in order to generate reasonable surface winds and evaporation as compared to observational products as shown in the supplemental material. The difference in roughness length between land and ocean for momentum is reasonable as compared to observations (table 8 of Wiernga 1993). The magnitude of the reduction in the roughness length for moisture exchange over land that we impose is, on the face, unrealistic (Beljaars and Holtslag 1991). However, the resulting difference in the drag coefficient between land and ocean used by Monin-Obukhov similarity theory is approximately a factor of 4.5 for momentum and 0.75 for moisture, and it is the drag coefficients that actually affect the large-scale flow. If anything, the resulting reduction in moisture availability over land is not strong enough, and precipitation and evaporation biases are still present over desert regions (see the supplement).

The heat capacity for oceanic grid points is set to $4 \cdot 10^8\ JK^{-1}m^{-2}$ (equivalent to a mixed layer depth of 100m), and for land grid points, to $8 \cdot 10^6\ JK^{-1}m^{-2}$ (equivalent to a mixed layer depth of 2m). For experiments with no land-sea contrast the oceanic mixed layer depth is used everywhere.

For experiments with land-sea contrast, we set the albedo as

$$\text{albedo} = 0.27 + \frac{0.75-0.27}{2} \cdot \left[1+\tanh\left(\frac{\phi-75^\circ}{5^\circ}\right)\right] + \frac{0.75-0.27}{2} \cdot \left[1-\tanh\left(\frac{\phi+70^\circ}{5^\circ}\right)\right] \quad (1)$$

which leads to higher albedo values over the Arctic and Antarctic. Otherwise the albedo is set to 0.27 everywhere. MiMA has no clouds, and this albedo was primarily tuned to approximate the shortwave effects of clouds.

b. Zonal asymmetries in the ocean

Ocean horizontal heat transport (often referred to as Q-fluxes in the modeling literature) is specified in order to force zonal asymmetries in surface temperatures following Jucker and Gerber (2017) so that the western part of oceanic basins are warmer than the eastern part. Merlis et al. (2013) and Jucker and Gerber (2017) specified a zonally uniform ocean horizontal heat transport as

$$\nabla \cdot \mathbf{F}_o(\phi) = Q_o \frac{1}{cos\phi}\left(1 - \frac{2\phi^2}{\phi_o^2}\right) exp\left(-\frac{\phi^2}{\phi_o^2}\right) \tag{2}$$

with Q_o=30W/m^2 and $\phi_o = 16°$ (repeated from equation 2 of Jucker and Gerber 2017; Merlis et al. 2013). All experiments here employ this meridional heat flux though we set Q_o=26W/m^2. Jucker and Gerber (2017) explored zonal heat transport by the ocean, and added an idealized warmpool. Here we implement a warmpool and an approximation of western boundary currents that more closely resemble those in nature, with the goal of capturing stationary waves as realistically as CMIP5 models.

The chosen representation of the Pacific warm pool is

$$\nabla \cdot \mathbf{F}_{\text{Pacific}}(\phi) = \begin{cases} (1-(\frac{\phi}{35°})^4)\cdot Q_{\text{Pacific}} \cdot \cos(5/3(\lambda - 150°)) & , \quad 96° \leq \lambda \leq 312° \text{ and } |\phi| < 35° \\ 0 & , \quad \text{otherwise} \end{cases} \tag{3}$$

An Atlantic "warmpool" is added analogously,

$$\nabla \cdot \mathbf{F}_{\text{Atlantic}}(\phi) = \begin{cases} (1-(\frac{\phi}{35°})^4)\cdot Q_{\text{Atlantic}} \cdot \cos(4(\lambda - 310°)) & , \quad 288° \leq \lambda \leq 18° \text{ and } |\phi| < 35° \\ 0 & , \quad \text{otherwise} \end{cases} \tag{4}$$

Note that both the Atlantic and Pacific warmpool anomalies add no net heat to the atmosphere, and merely redistribute heat zonally within the tropics. For experiments in which a warmpool is included, $Q_{\text{Pacific}} = 18$W/m^2 and $Q_{\text{Atlantic}} = 15$W/m^2. These values are chosen in order to capture as closely as possible the observed zonal asymmetry in sea surface temperature, though we slightly exaggerate the Atlantic temperature asymmetry in order to illustrate how weak an effect it has on stationary waves.

To approximate western boundary currents and the subtropical and extratropical ocean gyres, we redistribute heat in the extratropics as well. The goal is to capture zonal asymmetry in SSTs, not to accurately capture the meridional heat transport by the western boundary currents. The chosen representation of Gulf Stream and Kuroshio currents is as follows:

$$\nabla\cdot\mathbf{F}_{\mathrm{Gulf}}(\phi)=Q_{\mathrm{Gulf}}\cdot\left[\left(1-\left(\frac{\phi-37^\circ}{10^\circ}\right)^4\right)\cdot[A+B]+0.7\cdot\left(1-\left(\frac{\phi-67^\circ}{10^\circ}\right)^4\right)\cdot[C+D]\right] \tag{5}$$

where

$$A=\cos(4(\lambda-290.5^\circ)), 268^\circ\leq\lambda\leq358^\circ \text{and } 27^\circ<\phi<47^\circ \tag{6}$$

$$B=0.535\cdot\sin(8(\lambda-290.5^\circ)), 268^\circ\leq\lambda\leq313^\circ \text{and } 27^\circ<\phi<47^\circ \tag{7}$$

$$C=\cos(3(\lambda-348^\circ)), 258^\circ\leq\lambda\leq18^\circ \text{and } 57^\circ<\phi<77^\circ \tag{8}$$

$$D=0.25\cdot\cos(6(\lambda-288^\circ)), 243^\circ\leq\lambda\leq303^\circ \text{and } 57^\circ<\phi<77^\circ \tag{9}$$

$$\nabla\cdot\mathbf{F}_{\mathrm{Kuroshio}}(\phi)=Q_{\mathrm{Kuroshio}}\cdot\left(1-\left(\frac{\phi-37^\circ}{10^\circ}\right)^2\right)\cdot[E+F] \tag{10}$$

where

$$E=\cos(4(\lambda-155^\circ)), 132.5^\circ\leq\lambda\leq222.5^\circ \text{and } 27^\circ<\phi<47^\circ \tag{11}$$

$$F=-0.65\cdot\cos(6(\lambda-165^\circ)), 180^\circ\leq\lambda\leq240^\circ \text{and } 27^\circ<\phi<47^\circ \tag{12}$$

Terms A, B, ..., F are zero outside of the region indicated.

Similar to the imposed warmpools, the Kuroshio and Gulf Stream anomalies add no net heat to the atmosphere, and just flux heat from the eastern or central part of oceanic basins to the western parts. The poleward component of the Gulf Stream forcing (term C and term D) warms the Norwegian Sea and cools the Labrador Sea and adjacent areas in Northern Canada. For experiments in which western boundary oceanic heating is included, $Q_{\text{Gulf}} = 60\text{W/m}^2$ and $Q_{\text{Kuroshio}} = 25\text{W/m}^2$. Our representation of the Gulf and Kuroshio Currents are not intended to represent the small scale ocean frontal features, but rather to force a broad region of heating. No representation of Southern Hemisphere ocean heat fluxes, and specifically of the fluxes that help drive the South Pacific Convergence Zone, have been included. Therefore in this paper we focus on the Northern Hemisphere only.

c. Topography and additional details of the model forcing

Observed topography is used for the most realistic experiment, albeit at the resolution of the model with no effort to adjust the amplitude to preserve ridge heights (sometimes referred to as envelope topography). For experiments without topography, the topographic height over land areas is set uniformly to 15 meters. For code implementation reasons we do not use zero, but 15m is sufficient to suppress Rossby waves generated by topography. For simplicity we refer to all mountains in Central Asia as the Tibetan plateau, though we acknowledge that mountains further north near Mongolia may be more important for forcing stationary waves (White et al. 2017).

CO_2 is a scalar constant, set to 390 ppm throughout the atmosphere to roughly approximate concentrations during the period of the observational and reanalysis data we use to assess the model. In the simulations presented here, ozone is specified as the time and zonal mean of ozone specified for the CMIP5 forcing from 1850 through 1880 (Cionni et al. 2011); the ozone varies in latitude and pressure but not in longitude or time.

d. Experiments

Table 1 lists the 7 experiments included in this paper, each experiment lasting 38 years after discarding at least 10 years of spin-up. In addition to these seven experiments, Section 5 describes sensitivity experiments that explore the region in which ocean heat fluxes are most important for stationary waves. Section 5 also describes sensitivity experiments that assess the relative importance of three different elements of land-sea contrast: the difference in mechanical damping of near surface winds between the land and ocean, the difference in evaporation between land and ocean, and the difference in heat capacity. All integrations here were run at at a horizontal resolution of triangular truncation 42 (T42), though the most realistic configuration was also run at T84. All integrations were run with 40 vertical levels with a model lid near 70km.

To emphasize differences from previous idealized modeling studies, we note that this model does not use a stratospheric sponge layer, Rayleigh damping, or temperature relaxation of any kind. All damping on large scales is done by physically motivated processes, e.g., a gravity wave scheme for the middle atmosphere and Monin-Obukhov similarity theory for the surface layer, as in comprehensive general circulation models. Furthermore, we do not impose diabatic heating, but rather parameterize the underlying processes that influence diabatic heating. The surface temperature is not prescribed. Rather, it changes in response to changing surface fluxes of sensible heat, latent heat, and radiation. The novelty yet flexibility of this model allows us to dissect the building blocks of stationary waves more cleanly than has been done before.

The code will be made publicly available in MiMA release v2.0. The exact technical details and extensive parameter descriptions of MiMA release v1.0.1 can be found in the online documentation at https://mjucker.github.io/MiMA, and the key changes in MiMA relative to the model of Jucker and Gerber (2017) are documented above.

3. Stationary waves in MiMA

We now assess the fidelity of the stationary waves in the most realistic configuration of MiMA, which includes all relevant forcings (hereafter ALL, experiment 7 in Table 1). We begin with the stationary wave field in 300hPa geopotential height in MERRA reanalysis (Figure 1a) and ALL (Figure 1b), defined here as the deviation of the time averaged height field from its zonal mean. In both the model and in observations, lower heights are present over East Asia and the West Pacific and also over the Eastern United States, while higher heights are present over Western North America and Western Eurasia. The magnitude of the stationary wave field in MiMA is similar to that in observations in most regions, though somewhat weak over Europe and North America in winter.

There are biases in the stationary waves (e.g., over the North Atlantic), but we now show that stationary waves in MiMA as just as good as those in comprehensive general circulation models. The relative magnitude of 300hPa geopotential height stationary waves at 50N is quantified in Figure 2a for MERRA reanalysis (green), ALL (blue; integration 7 on Table 1), and 42 different CMIP5 models (thin lines). The biases in ALL are not any worse than those in many CMIP5 models, and MiMA lies well within the envelope of the CMIP5 models for nearly all longitudes.

Figure 3 is the same as Figure 2, but for the stationary waves at 50hPa. The stratospheric stationary waves in MiMA are nearly identical to those in reanalysis data, and markedly better than in most CMIP5 models. During wintertime, stationary eddies couple with the stratosphere (Wang and Kushner 2011), which has been shown to affect the north-south position of the Atlantic storm track (Shaw et al. 2014). Additional discussion of the realism of the mean state of MiMA is included in the supplemental material.

To address the sampling uncertainty in the stationary waves, we compute averages for the first 19 and last 19 years of the 38-year long ALL integration separately, and show the stationary waves in orange lines on Figure 2b. The blue ALL line is repeated from Figure 2a. For most of the NH the blue line is not visible because of the close correspondence with the two orange lines.

The results are also not sensitive to the horizontal resolution. Figure 1c shows the stationary wave pattern in an experiment performed at T84 resolution, and the stationary waves are quantitatively similar. The black line on Figure 2b shows the 50N stationary waves for the T84 ALL integration, and it is very close to the corresponding lines for T42 resolution. Therefore, for the remainder of this manuscript we focus on integrations performed at T42 resolution.

4. The (non)linearity of the stationary wave building blocks

We now use MiMA to probe the building blocks of stationary waves. We address each of the questions posed in the introduction separately.

a. Do the stationary waves in ALL equal the sum of the stationary wave response to each forcing?

We first consider whether the stationary wave pattern can be decomposed linearly into the various forcings. Figure 4a repeats the stationary wave pattern for ALL from Figure 1b, and Figure 4b shows the sum of the stationary wave patterns in the topography only, ocean heat fluxes only, and land-sea contrast only experiments (i.e., the stationary waves are calculated for each integration separately and then summed). While the stationary wave field over Europe in ALL appears to be associated with the linear summation of the forcings, the stationary wave field over the Pacific is not. First, the low over East Asia and the West Pacific is approximately 30% stronger in ALL than when the individual forcings are summed. Even larger discrepancies are evident over the Northeast Pacific and Western North America: there is no ridge when each forcing is imposed in isolation, while ALL simulates a ridge in this region as observed (Figure 1a). Finally, the ridge over Western Siberia is stronger when each forcing is imposed in isolation than in ALL. Overall, the stationary waves in ALL do not resemble a simple linear summation of the individual response to each forcing over much of the Northern Hemisphere.

The non-additive behavior is summarized in Figure 2b. The blue curve in Figure 2b repeats the stationary wave pattern in ALL for geopotential height at 300hPa and 50N, and the gray shading repeats the spread in the 42 CMIP5 models. Figure 2b adds on experiments with topography only, ocean heat fluxes only, and land-sea contrast only, and the dotted blue line in Figure 2b is the sum of the stationary waves for these three individual forcing experiments. In the Pacific sector, the summed response to the individual forcings is weaker than the response when all forcings are imposed together (substantial nonlinearities in this region have been noted before, e.g., Held et al. 2002). In the Atlantic sector, however, linearity is a reasonable assumption. Over the Atlantic and European sectors land-sea contrast plays the largest role, and topography plays a larger role further to the east over Western Russia. Orography is the most important factor for Pacific storm tracks, though land-sea contrast has a non-negligible role. Note, however, that one must be cautious in ranking the relative importance of the factors if the forcings interact nonlinearly as they do in the Pacific sector.

Figure 3b is similar to Figure 2b but for the stationary waves at 50hPa. No single forcing dominates the generation of stratospheric stationary waves, though orography (red) is seemingly most important (largely consistent with Inatsu et al. 2002). The sum of the stratospheric responses to each individual forcing is quantitatively similar to the response in ALL in the Eastern Hemisphere, though not in the Western Hemisphere where the magnitude is weaker in the North American sector and stronger over the Atlantic. The net stationary wave field in ALL has a stronger (weaker) zonal wavenumber 2 (1) component than the sum of the stratospheric responses to each individual forcing.

Zonal asymmetries in surface temperatures are also non-additive in response to each of the three forcings. Figure 2c shows the zonal asymmetries in surface temperatures in ALL, topography only, ocean heat fluxes only, and land-sea contrast only, and the dotted blue line in Figure 2c is the sum of the zonally asymmetric component of surface temperature for these three individual forcing experiments. Over the Eastern Atlantic and Western Europe surface temperatures are up to 1.7K warmer in ALL than in linear sum of the response to each forcing. In this region land-sea contrast is the dominant forcing due to the thermal inertia of the Atlantic Ocean from summer to winter, though topography contributes up to $\sim 1.8K$ of warming in this region. Eastern Canada is 3.5K colder in ALL than in the simple linear summation of the response to ocean heat fluxes only, land-sea contrast only, and topography only, and results are similar at 40N over the Eastern United States (not shown). While land-sea contrast is the strongest individual forcing in this region, the substantial difference between ALL and the sum of the individual responses highlights the non-linearities that govern surface temperatures. These results support those of Brayshaw et al. (2009) and Seager et al. (2002) who highlight the importance of the Rocky Mountains in generating stationary waves that enhance the temperature difference between the eastern and western margins of the North Atlantic.

b. Which forcings interact non-additively?

We now explore why the stationary wave pattern in ALL differs from the summation of the response to each forcing applied individually. Specifically, which forcings are most responsible for the non-additive behavior evident in Section 4a? Before proceeding we review the definition of the isolated and full nonlinear response of Held et al. (2002). The response to some source of asymmetry A in MiMA can be denoted as $M(A)$, and let F represent all three forcings in the most realistic configuration such that the response to F is $M(F)$. As in Held et al. (2002), we refer to $M(A)$ as the isolated nonlinear response to A and $M(F)$ - $M(F$ - $A)$ as the full nonlinear response to A. If we consider adding the different parts of the forcing in sequence, the isolated nonlinear response to A occurs when A is added first, while the full nonlinear response to A occurs when A is added last (or is the first to be removed).

The bottom three rows of Figure 4 show the stationary wave response to each forcing imposed in isolation (right column; *isolated nonlinear response*) and also when each forcing is removed from ALL (left column; the *full nonlinear response*). For example, Figure 4c considers the difference in stationary waves between ALL and the experiment where both land-sea contrast and topography are imposed but ocean heat flux zonal asymmetry is not. Hence, the stationary wave pattern in Figure 4c is that forced by ocean heat flux zonal asymmetries when imposed on a basic state that already includes land-sea contrast and topography (the *full nonlinear response*). This pattern in Figure 4c can be compared to the *isolated nonlinear* response to ocean heat flux zonal asymmetries in Figure 4d. Ocean heat flux zonal asymmetries in isolation have a limited impact on the Pacific sector stationary wave pattern, but when imposed on the basic state set up by topography and land-sea contrast the effect more than doubles in strength (consistent with Blackmon et al. 1987, among others). Note that zonal asymmetries in ocean heat fluxes have a minimal effect on European stationary waves. Section 4c will provide a diagnostic accounting for this difference between the isolated nonlinear and full nonlinear responses.

Figure 4e shows the impact that land-sea contrast has on stationary waves when imposed on a basic-state that already includes topography and E-W zonal asymmetries, while Figure 4f shows the isolated nonlinear response. Over Europe the full nonlinear and isolated nonlinear responses are similar, though the full nonlinear response is stronger. In contrast, over the Pacific sector they differ qualitatively, with only the full nonlinear response indicating a trough over the West Pacific and a ridge over the west coast of North America.

Finally, Figure 4g shows the full nonlinear response to topography, while Figure 4h shows the isolated nonlinear response to topography. Over Eurasia the full nonlinear response is weaker than the isolated nonlinear response. In contrast, the full nonlinear response to the Rockies is stronger than the isolated nonlinear response. Only over the Northwest Pacific are the isolated nonlinear and full nonlinear responses similar.

In summary, there are four key differences between the isolated nonlinear and full nonlinear responses: (i) land-sea contrast and (ii) ocean heat flux asymmetries have a weaker impact on the Northwest Pacific low in isolation as compared to the full nonlinear response, (iii) the response to the Rockies is weaker in isolation as compared to the full nonlinear response, while (iv) the response to the Tibetan Plateau is stronger in isolation as compared to the full nonlinear response. These four nonlinearities, as well as additional weaker instances, are summarized in Table 2.

c. Why do the isolated nonlinear and full nonlinear responses differ?

The goal of this subsection is to explain why the isolated nonlinear and full nonlinear responses differ. First, we introduce the zonally anomalous steady-state thermodynamic balance, our main tool for explaining these differences. We then evaluate all terms in the budget for ALL in order to establish context. Next, we utilize the budget to explain the differences between the full nonlinear and isolated nonlinear responses. Finally, we consider whether other budgets provide additional insight into the difference between the isolated nonlinear and full nonlinear responses.

The zonally anomalous steady-state thermodynamic balance can be written as (equation 11 of Wills and Schneider 2018)

$$\left(\overline{u}\frac{\partial\overline{\theta}}{\partial x}+\overline{v}\frac{\partial\overline{\theta}}{\partial y}+\overline{\omega}\frac{\partial\overline{\theta}}{\partial p}\right)^{*}+\nabla\cdot(\overline{\mathbf{v}'\theta'})^{*}-\overline{Q}^{*}=0 \tag{13}$$

Here, θ is the potential temperature, ω is the vertical pressure velocity, and Q is the diabatic heating due to latent heat release, radiation, and other non-conservative processes. Time means are denoted with a bar. Deviations from a zonal average are denoted by $*$, and deviations from a time average are denoted by primes, such that $\nabla\cdot(\mathbf{v}'\theta')*$ is the zonally anomalous potential-temperature-flux divergence by transient eddies. The basic state temperature gradient plays a large role for this budget, and we therefore show in Figure 5 the zonally asymmetric 300hPa temperature field onto which the forcings are added. In ALL, pronounced zonal asymmetries in temperature are present with the western coasts of continents warmer than the eastern coasts in midlatitudes. All three forcings are important for this structure.

We consider all terms in the budget 13 for ALL in Figure 6 in order to establish how the various terms combine for a nearly closed budget. Zonal advection (Figure 6a) leads to strong cooling exceeding 10K/day off the coast of East Asia, and warming of up to 4K/day over Western North America. These temperature tendencies are due to the advection of strong zonal temperature gradients by westerly winds (Figure 5a) in these regions. In addition, to the east of the Rockies and Tibetan plateau, where subsidence occurs, there is a warming tendency due to the vertical term (Figure 6c). The diabatic heating and eddy heat flux terms are small (the implications of this are discussed in the Discussion section), and the meridional advection term completes the budget (Figure 6b). In particular, there is southward advection of cold air over East Asia and northward advection of warm air over the Western Pacific associated with the trough in the far Western Pacific. Similarly, over North America, the vertical term leads to cooling over the West Coast and warming over the Plains region, while the zonal advection leads to warming over the western third of the continent. These temperature tendencies are balanced by the meridional temperature advection associated with the ridge over the Rockies. Residuals are large only over topography (Figure 6f), where the interpolation from the model hybrid vertical coordinate to pressure coordinates impacts the wind and temperature field.

We now use this budget in order to clarify why the isolated nonlinear and full nonlinear responses to individual building blocks differ. To aid in our interpretation of how the zonally anomalous steady-state thermodynamic balance can be used to illuminate the forcing of stationary waves, we re-arrange budget 13 as

$$\left(\overline{v}\frac{\partial\overline{\theta}}{\partial y}\right)^{*} = \overline{Q}^{*} - \left(\overline{u}\frac{\partial\overline{\theta}}{\partial x} + \overline{\omega}\frac{\partial\overline{\theta}}{\partial p}\right)^{*} - \nabla\cdot(\overline{\mathbf{v}'\theta'})^{*} \tag{14}$$

Terms on the right-hand side are interpreted here as forcings that must be balanced by changes in $\overline{v}$ (see section 3 of Hoskins and Karoly (1981) and section 4a of Inatsu et al. (2002)). If the sum of the terms on the right-hand-side is negative, then warm air must be advected from more tropical latitudes in order to balance the budget, requiring southerly winds. On the other hand if the sum of the terms on the right-hand-side is positive, then cold air must be advected from more poleward latitudes in order to balance the budget, requiring northerly winds.

We first address why both land-sea contrast and ocean heat fluxes have a weaker impact on the Northwest Pacific low in the isolated nonlinear response as compared to the full nonlinear response (Figure 4e vs. 4f and Figure 4g vs. 4h). Figure 7, 8 , and 9 show the meridional advection term, zonal advection term, and vertical term for the isolated nonlinear and full nonlinear responses for each forcing. Meridional advection leads to a cooling tendency near Japan and a warming tendency over the Central Pacific (Figure 7c and Figure 7e), but such a response is far weaker in the isolated nonlinear response (compare Figure 7c to Figure 7d and Figure 7e to Figure 7f).

This change in magnitude of meridional advection is consistent with the difference in strength of the low off the coast of Asia (Figure 4), as the meridional winds associated with this low cause this meridional temperature advection. The meridional temperature advection is balanced by the zonal advection term (Figure 8c, and Figure 8e): the stronger Northwest Pacific winds associated with ocean heat flux asymmetries and land-sea contrast advect colder continental temperatures off the coast of Asia if East Asia is already cold. The background state of 300hPa temperature zonal gradients are shown in Figure 5ef, and include a cold continental East Asia in winter. These cold temperatures are due to the effect of the Tibetan Plateau, as even if topography is imposed in isolation temperatures are colder over East Asia (Figure 5c). [1]. The net effect is that the meridional temperature advection term must be larger in the full nonlinear response than in the isolated nonlinear response for a closed steady-state budget, and this in turn necessitates a stronger trough in the full nonlinear response.

Why is the response to the Rockies weaker in the isolated nonlinear response as compared to the full nonlinear response (Figure 4c vs. 4d)? The zonally anomalous steady-state thermodynamic balance can again provide a diagnosis of this effect. Meridional advection leads to cooling over the Plains and warming over the far-Northeastern Pacific (Figure 7g and Figure 7h), but such a response is far weaker in the isolated nonlinear response in Figure 7h. This dipolar meridional advection is associated with the ridge over the Rockies, which is stronger in the full nonlinear response. The vertical term is similar in the isolated nonlinear and full nonlinear response, and hence does not account for this difference (Figure 9g and Figure 9h). Rather, the meridional temperature advection is balanced by the zonal advection term (Figure 8g, and Figure 8h): land-

[1]The vertical term also is associated with warmer of the East Coast of Asia and cooling over the Western Pacific (Figure 9c and Figure 9e) that is more pronounced in the full nonlinear response, though we interpret this warming of the East Coast of Asia as the subsidence located to the west of a low in quasi-geostrophic theory, and the low is stronger in the full nonlinear response.

sea contrast leads to a large gradient in temperatures between the East Pacific and North America (Figure 5d), and hence there is a warming tendency over Western North America. A stronger stationary wave response must exist in order to balance this warming through enhanced meridional advection.

The thermodynamic budget does not appear to explain why the full nonlinear response to topography is weaker over Western Russia. This effect can be more directly explained by examining the lower tropospheric winds incident on the mountains of Central Asia when topography is imposed on a zonally symmetric background state versus a background state that already incorporates land-sea contrast. When land-sea contrast is included, the surface winds incident on the Tibetan Plateau are weaker due to enhanced surface drag than when land-sea contrast is not included; for example, 850hPa zonal wind at 40N, 65E are 12.0m/s in the no-forcing integration (experiment 0 in Table 1) and 8.1m/s in the integration with ocean heat flux asymmetry and land-sea contrast; the differences in 850hPa zonal wind at 45N, 65E and 50N, 65E are even larger: 4.9m/s and 4.5m/s respectively. These weaker winds incident on the mountains of Central Asia lead to weaker low-level rising motion and hence a weaker stationary wave response.

Finally, we have also computed the Rossby wave source as in Sardeshmukh and Hoskins (1988) for each experiment, and the results are shown in Figure 10. The Rossby wave source in ALL is similar to that in the linear summation except over East Asia/Tibetan Plateau and the far West Pacific, where the anomalies in ALL are stronger. The Rossby wave source in the far Western Pacific is stronger for the full nonlinear response to both east-west asymmetries and land sea contrast as compared to the isolated nonlinear response, and hence is consistent with the stronger stationary wave response (Figure 4e vs. 4f and Figure 4g vs. 4h). We can decompose the change in Rossby wave source into the the advection of absolute vorticity by the divergent wind ($-\mathbf{v}_\chi \cdot (\zeta + f)$) and the direct forcing by divergence ($(\zeta + f)\nabla \cdot \mathbf{v}$). The latter term dominates, but the former term acts as a non-negligible negative feedback (not shown). Indeed the pattern of upper level divergence (Figure S1) exhibits enhanced divergence in the subtropical far-western Pacific for the full nonlinear response to east-west asymmetry and land-sea contrast as compared to the isolated nonlinear response (Figure S1c versus S1d, and Figure S1e versus S1f).

The Rossby wave source over the Rockies differs between the isolated nonlinear and full nonlinear response to topographic forcing (Figure 10gh), and appears to act as a negative feedback as divergence over the West Coast of North America is stronger in the isolated nonlinear response (Figure S1gh); the dynamics of this feature should be explored for future work. We have also examined the generation of stationary waves using the Plumb (1985) wave activity fluxes, and while the amplitude of the fluxes differed between the isolated nonlinear and full nonlinear responses consistent with the amplitude of the stationary waves, there was no clear explanation of why such a difference may occur (not shown).

Overall, the thermodynamic budget, and to a lesser degree the Rossby wave source, allow us to diagnose why the isolated nonlinear and full nonlinear responses differ in response to each forcing. In all cases, the difference between the isolated nonlinear and full nonlinear response can be tracked down to differences in the background state set up by the other forcings upon which a new forcing is added.

5. Sensitivity analysis for land-sea contrast and east-west asymmetry

We now explore which aspect of east-west asymmetry in ocean heat fluxes is most important for stationary waves. Figure 11a shows the eddy height field at 300hPa and 50N similar to Figure 2 for the isolated nonlinear response to the Pacific warm pool (green in Figure 11a), the isolated nonlinear and full nonlinear response to all E-W asymmetries except the Pacific warm pool (black and gray in Figure 11a respectively), and also in which a Pacific warm pool is added to a model configuration with land-sea contrast and topography (light blue in Figure 11a). The solid blue line is ALL, and the magenta line is repeated from Figure 2. Over the Pacific sector, the green and magenta lines are nearly identical and both the isolated nonlinear and full nonlinear response to ocean heat fluxes in other sectors is small. Hence, the Pacific warm pool is the most important contributor to the stationary waves forced by ocean heat fluxes in the Pacific sector. In the Atlantic sector, the Pacific warm pool is comparatively unimportant (as the green line is generally closer to zero than the magenta line), though differences between the isolated nonlinear and full nonlinear responses to individual forcings preclude a simple interpretation as to which zonal asymmetries in ocean heat fluxes are most important.

Which aspect of land-sea contrast is most important for forcing the stationary wave pattern? Recall that we include three aspects in ALL: the difference in mechanical damping of near surface winds between the relatively rough land surface and relatively smooth ocean, the difference in evaporation between land and ocean, and the difference in heat capacity. Figure 11b is constructed in a similar manner to Figure 11a, and attempts to answer this question by considering the full and isolated nonlinear responses to these three components. The isolated nonlinear response and full nonlinear responses the combined effect of heat capacity and evaporation differences between land and ocean are shown in orange and red respectively; the isolated and full nonlinear responses differ strongly. Black and gray lines shown the isolated nonlinear response and full nonlinear response to land-ocean differences in damping of wind, and as in the orange and red lines there are qualitative differences between the isolated and full nonlinear responses. Hence the response to the various components of land-sea contrast differ depending on the order in which they are introduced. Stated another way, if the isolated nonlinear stationary wave response to heat capacity and evaporation (in orange) is added to the isolated nonlinear stationary wave response to roughness for mechanical dissipation (in black), one does not recover the isolated nonlinear stationary wave response when all three forcings are included (cyan, repeated from Figure 2). We therefore are unable to draw conclusions as to which aspect of land-sea contrast is most important.

6. Discussion and Conclusions

A good understanding of the mechanisms controlling stationary waves is important. First, the position and intensity of stationary waves strongly influence surface temperatures over populated midlatitude regions, modifying the direction of winds and hence temperature advection. Second, stationary waves influence the distribution of storm tracks and their associated extreme wind and precipitation events. Subtle shifts in the stationary waves can therefore lead to profound impacts on regional climate even if zonally averaged changes are small. To interpret and have confidence in simulated changes in the regional climate of the extratropics, it is important to have a good understanding of mechanisms for stationary waves.

Can one reconstruct the full magnitude of stationary waves by adding together the individual building blocks? In the Pacific sector, the answer is resolutely no. Over the Northwest Pacific/East Asia, the sum of the responses to each individual forcing is $\sim 30\%$ weaker as compared to a simulation in which all three forcings are included and interact with one-another. Over the Northeast Pacific and North America, the sum of the responses to each forcing is actually opposite to that when all three are imposed simultaneously. Only over Western Eurasia is additivity a reasonable assumption. This leads to stratospheric stationary waves that are similarly non-additive in the Western Hemisphere. Surface temperature zonal asymmetries are also non-additive over Europe and North America.

The nonadditivity of the forcings over the Pacific sector is due to nonlinear interactions between the forcings. Specifically, the response to land-sea contrast and east-west ocean heat fluxes is qualitatively different if they are imposed on a basic state in which topography is already included.

Similarly, the response to topography is qualitatively different if it is imposed on a basic state in which land-sea contrast and east-west ocean heat fluxes are already included. The causes of this nonadditivity can be diagnosed using the zonally anomalous steady-state thermodynamic balance, and we find that the background state temperature field set up by each forcing (and especially the zonal derivatives of the temperature field) play a crucial role in determining the strength (or even existence) of a stationary wave response to a given forcing. All three forcings considered here strongly impact the temperature field and its zonal gradients.

Despite the non-additivity of the various forcings, there are some regions where a single forcing plays the dominant role. For example, orography is the single most important factor for Pacific sector stationary wave, while over the European sector land-sea contrast plays a larger role. While the responses to each forcing are generally additive over Europe, there are still some ambiguities even in this region. For example, if land-sea differences in momentum drag are imposed in isolation on a zonally symmetric background state, then the response is minimal and one would interpret differential momentum drag as being unimportant. However if differential momentum drag is imposed on a background state already disturbed by orography and E-W ocean heat fluxes, then the response is nearly as strong as the full response to land-sea contrast. Such non-additivity implies that it is not possible to rank the relative importance of the factors in a robust manner.

In the zonally anomalous steady-state thermodynamic balance, the diabatic heating term was not found to be an important contributor to the generation of stationary waves. While at face value this may seem contrary to studies which imposed diabatic heating directly and found a strong response, we want to emphasize that diabatic is still crucial for the generation of stationary waves even in the context of the thermodynamic balance (albeit in an indirect manner). Namely, diabatic heating helps set up the large scale temperature and wind field critical for the response to the other forcing(s); specifically, diabatic heating leads to the difference between 5b and the other panels on

Figure 5. Specifically, the difference between the isolated nonlinear and full nonlinear response to e.g., topography over Western North America can be thought of as due to the diabatic heating pattern associated with land-sea contrast and east-west ocean heat fluxes. Similarly, eddy fluxes were found to be a negligible contributor to the generation of stationary waves in the zonally anomalous steady-state thermodynamic balance, but to the extent that eddy fluxes are important in setting up the large scale temperature and jet structure, they also indirectly control stationary waves.

Our results have implications for studies using a linear stationary wave model. Specifically, many of these studies find substantial sensitivity as to the details of the background state about which one linearizes (see the discussion in Held et al. 2002). In our nonlinear MiMA simulations we find that the Pacific sector stationary wave pattern is highly nonlinear, as a pre-existing background zonal temperature gradient allows for a qualitatively different response to a given forcing. Hence it is not surprising that a stationary wave model linearized about subtly different background states can produce qualitatively different stationary wave patterns.

While the experiments performed here help inform our understanding of the atmospheric response to imposed boundary conditions, the details of how the boundary conditions are imposed are imperfect. We do not explicitly resolve oceanic dynamics, and hence the heat transport from one oceanic region to another is imposed in an idealized manner. Specifically the fine-scale structure of the Kuroshio and Gulf currents are not imposed here, and it is conceivable that the inclusion of small scale SST gradients may modify our results. Furthermore, the evaporation in our most realistic configuration is still too large over many continental regions, especially over deserts. Lastly, the model also lacks clouds, and hence zonal asymmetries in cloud radiative fluxes are missing. There are still biases in the stationary waves in our most realistic configuration, when compared to observations. Despite these deficiencies, we want to emphasize the potential advantages of this model for scientific problems that require an idealized model with reasonable stationary waves. The model simulates stationary waves as realistic as those present in CMIP5 models, yet is flexible enough to allow for no stationary waves at all. The model also is relatively computationally inexpensive. Hence this model can be used to demonstrate that stationary waves on Earth are composed of building blocks that interact nonlinearly with one another, with the most pronounced non-additivity evident over the Pacific and North American sectors.

Acknowledgments. CIG, IW, and ME acknowledge the support of a European Research Council starting grant under the European Union Horizon 2020 research and innovation programme (grant agreement number 677756). EPG acknowledges support from the US NSF through grant AGS 1546585. MJ acknowledges support from the Australian Research Council (ARC) Centre of Excellence for Climate Extremes (CE170100023) and ARC grant FL 150100035.

References

Alexander, M., and T. Dunkerton, 1999: A spectral parameterization of mean-flow forcing due to breaking gravity waves. *Journal of the atmospheric sciences*, **56 (24)**, 4167–4182, doi:10.1175/1520-0469(1999)056⟨4167:ASPOMF⟩2.0.CO;2.

Beljaars, A., and A. Holtslag, 1991: Flux parameterization over land surfaces for atmospheric models. *Journal of Applied Meteorology*, **30 (3)**, 327–341.

Betts, A., and M. Miller, 1986: A new convective adjustment scheme. part ii: Single column tests using gate wave, bomex, atex and arctic air-mass data sets. *Quarterly Journal of the Royal Meteorological Society*, **112 (473)**, 693–709, doi:10.1002/qj.49711247308.

Betts, A. K., 1986: A new convective adjustment scheme. part i: Observational and theoretical basis. *Quarterly Journal of the Royal Meteorological Society*, **112 (473)**, 677–691, doi:10.1002/

qj.49711247307.

Blackmon, M. L., G. W. Branstator, G. T. Bates, and J. E. Geisler, 1987: An analysis of equatorial pacific sea surface temperature anomaly experiments in general circulation models with and without mountains. *Journal of the atmospheric sciences*, **44 (14)**, 1828–1844.

Bracegirdle, T. J., E. Shuckburgh, J.-B. Sallee, Z. Wang, A. J. Meijers, N. Bruneau, T. Phillips, and L. J. Wilcox, 2013: Assessment of surface winds over the atlantic, indian, and pacific ocean sectors of the southern ocean in cmip5 models: Historical bias, forcing response, and state dependence. *Journal of Geophysical Research: Atmospheres*, **118 (2)**, 547–562.

Branstator, G., 1995: Organization of storm track anomalies by recurring low-frequency circulation anomalies. *Journal of the atmospheric sciences*, **52 (2)**, 207–226.

Brayshaw, D. J., B. Hoskins, and M. Blackburn, 2009: The basic ingredients of the north atlantic storm track. part i: Land–sea contrast and orography. *Journal of the Atmospheric Sciences*, **66 (9)**, 2539–2558.

Brayshaw, D. J., B. Hoskins, and M. Blackburn, 2011: The basic ingredients of the north atlantic storm track. part ii: Sea surface temperatures. *Journal of the Atmospheric Sciences*, **68 (8)**, 1784–1805.

Broccoli, A. J., and S. Manabe, 1992: The effects of orography on midlatitude northern hemisphere dry climates. *Journal of Climate*, **5 (11)**, 1181–1201.

Chang, E. K., 2009: Diabatic and orographic forcing of northern winter stationary waves and storm tracks. *Journal of Climate*, **22 (3)**, 670–688.

Chang, E. K., S. Lee, and K. L. Swanson, 2002: Storm track dynamics. *Journal of climate*, **15 (16)**, 2163–2183.

Charney, J. G., and A. Eliassen, 1949: A numerical method for predicting the perturbations of the middle latitude westerlies. *Tellus*, **1 (2)**, 38–54.

Cionni, I., and Coauthors, 2011: Ozone database in support of cmip5 simulations: results and corresponding radiative forcing. *Atmospheric Chemistry and Physics*, **11 (21)**, 11 267–11 292.

Cohen, N. Y., E. P. Gerber, and E. P. Oliver Bühler, 2013: Compensation between resolved and unresolved wave driving in the stratosphere: Implications for downward control. *Journal of the Atmospheric Sciences*, **70 (12)**, 3780–3798, doi:10.1175/JAS-D-12-0346.1.

Frierson, D. M., I. M. Held, and P. Zurita-Gotor, 2006: A gray-radiation aquaplanet moist gcm. part i: Static stability and eddy scale. *Journal of the atmospheric sciences*, **63 (10)**, 2548–2566, doi:10.1175/JAS3753.1.

Frierson, D. M., I. M. Held, and P. Zurita-Gotor, 2007: A gray-radiation aquaplanet moist gcm. part ii: Energy transports in altered climates. *Journal of the atmospheric sciences*, **64 (5)**, 1680–1693, doi:10.1175/JAS3913.1.

Held, I. M., 2005: The gap between simulation and understanding in climate modeling. *Bulletin of the American Meteorological Society*, **86 (11)**, 1609–1614.

Held, I. M., and M. Ting, 1990: Orographic versus thermal forcing of stationary waves: The importance of the mean low-level wind. *Journal of the Atmospheric Sciences*, **47 (4)**, 495–500.

Held, I. M., M. Ting, and H. Wang, 2002: Northern winter stationary waves: Theory and modeling. *Journal of climate*, **15 (16)**, 2125–2144.

Hoskins, B. J., and D. Karoly, 1981: The steady linear response of a spherical atmosphere to thermal and orographic forcing. *J. Atmos. Sci.*, **38**, 1179–1196.

Hu, Y., and K. K. Tung, 2002: Tropospheric and equatorial influences on planetary-wave amplitude in the stratosphere. *Geophys. Res. Lett.*, **29 (2)**, 1019, doi:10.1029/2001GL013762.

Iacono, M. J., E. J. Mlawer, S. A. Clough, and J.-J. Morcrette, 2000: Impact of an improved longwave radiation model, rrtm, on the energy budget and thermodynamic properties of the ncar community climate model, ccm3. *Journal of Geophysical Research: Atmospheres*, **105 (D11)**, 14 873–14 890.

Inatsu, M., H. Mukougawa, and S.-P. Xie, 2002: Stationary eddy response to surface boundary forcing: Idealized gcm experiments. *Journal of the atmospheric sciences*, **59 (11)**, 1898–1915.

Jucker, M., and E. Gerber, 2017: Untangling the annual cycle of the tropical tropopause layer with an idealized moist model. *Journal of Climate*, **30 (18)**, 7339–7358.

Kaspi, Y., and T. Schneider, 2013: The role of stationary eddies in shaping midlatitude storm tracks. *Journal of the atmospheric sciences*, **70 (8)**, 2596–2613.

Kitoh, A., 1997: Mountain uplift and surface temperature changes. *Geophysical research letters*, **24 (2)**, 185–188.

Manabe, S., and T. B. Terpstra, 1974: The effects of mountains on the general circulation of the atmosphere as identified by numerical experiments. *Journal of the atmospheric Sciences*, **31 (1)**, 3–42.

Merlis, T. M., T. Schneider, S. Bordoni, and I. Eisenman, 2013: Hadley circulation response to orbital precession. part ii: Subtropical continent. *Journal of Climate*, **26 (3)**, 754–771.

Mlawer, E. J., S. J. Taubman, P. D. Brown, M. J. Iacono, and S. A. Clough, 1997: Radiative transfer for inhomogeneous atmospheres: Rrtm, a validated correlated-k model for the longwave. *Journal of Geophysical Research: Atmospheres*, **102 (D14)**, 16 663–16 682.

Neelin, J. D., B. Langenbrunner, J. E. Meyerson, A. Hall, and N. Berg, 2013: California winter precipitation change under global warming in the coupled model intercomparison project phase 5 ensemble. *Journal of Climate*, **26 (17)**, 6238–6256.

Plumb, R. A., 1985: On the three-dimensional propagation of stationary waves. *Journal of the Atmospheric Sciences*, **42 (3)**, 217–229.

Ringler, T. D., and K. H. Cook, 1999: Understanding the seasonality of orographically forced stationary waves: Interaction between mechanical and thermal forcing. *Journal of the atmospheric sciences*, **56 (9)**, 1154–1174.

Sardeshmukh, P. D., and B. J. Hoskins, 1988: The generation of global rotational flow by steady idealized tropical divergence. *J. Atmos. Sci.*, **45**, 1228–1251.

Saulière, J., D. J. Brayshaw, B. Hoskins, and M. Blackburn, 2012: Further investigation of the impact of idealized continents and sst distributions on the northern hemisphere storm tracks. *Journal of the Atmospheric Sciences*, **69 (3)**, 840–856.

Seager, R., D. S. Battisti, J. Yin, N. Gordon, N. Naik, A. C. Clement, and M. A. Cane, 2002: Is the gulf stream responsible for europe's mild winters? *Quarterly Journal of the Royal Meteorological Society*, **128 (586)**, 2563–2586.

Shaw, T., and Coauthors, 2016: Storm track processes and the opposing influences of climate change. *Nature Geoscience*, **9 (9)**, 656.

Shaw, T. A., J. Perlwitz, and O. Weiner, 2014: Troposphere-stratosphere coupling: Links to north atlantic weather and climate, including their representation in cmip5 models. *Journal of Geophysical Research: Atmospheres*, **119 (10)**, 5864–5880.

Simpson, I. R., R. Seager, M. Ting, and T. A. Shaw, 2016: Causes of change in northern hemisphere winter meridional winds and regional hydroclimate. *Nature Climate Change*, **6 (1)**, 65.

Smagorinsky, J., 1953: The dynamical influence of large-scale heat sources and sinks on the quasi-stationary mean motions of the atmosphere. *Quarterly Journal of the Royal Meteorological Society*, **79 (341)**, 342–366.

Wang, L., and P. J. Kushner, 2011: Diagnosing the stratosphere-troposphere stationary wave response to climate change in a general circulation model. *Journal of Geophysical Research: Atmospheres*, **116 (D16)**.

White, R., D. Battisti, and G. Roe, 2017: Mongolian mountains matter most: Impacts of the latitude and height of asian orography on pacific wintertime atmospheric circulation. *Journal of Climate*, **30 (11)**, 4065–4082.

Wiernga, J., 1993: Representative roughness parameters for homogeneous terrain. *Boundary-Layer Meteorology*, **63 (4)**, 323–363.

Wills, R. C., and T. Schneider, 2018: Mechanisms setting the strength of orographic rossby waves across a wide range of climates in a moist idealized gcm. *Journal of Climate*, **31 (18)**, 7679–7700.

Wilson, C., B. Sinha, and R. G. Williams, 2009: The effect of ocean dynamics and orography on atmospheric storm tracks. *Journal of Climate*, **22 (13)**, 3689–3702.

Wu, Z., and T. Reichler, 2018: Towards a more earth-like circulation in idealized models. *Journal of Advances in Modeling Earth Systems*, doi:10.1029/2018MS001356.

Zappa, G., L. C. Shaffrey, and K. I. Hodges, 2013: The ability of cmip5 models to simulate north atlantic extratropical cyclones. *Journal of Climate*, **26 (15)**, 5379–5396.

LIST OF TABLES

TABLE 1. MiMA Experiments, with "Y" indicating a forcing is on and "N" indicating a forcing is off. The isolated nonlinear response to topography can be deduced from experiment 1, while the full nonlinear response is the difference between experiments 7 and 6. The isolated nonlinear response to land-sea contrast can be deduced from experiment 2, while the full nonlinear response is the difference between experiments 7 and 4. The isolated nonlinear response to ocean heat fluxes can be deduced from experiment 3, while the full nonlinear response is the difference between experiments 7 and 5.

Table: MiMA Model experiments

	orography	land-sea contrast	ocean heat fluxes
exp 0	N	N	N
exp 1	Y	N	N
exp 2	N	Y	N
exp 3	N	N	Y
exp 4	Y	N	Y
exp 5	Y	Y	N
exp 6	N	Y	Y
exp 7 (ALL)	Y	Y	Y

TABLE 2. Summary of nonlinearities.

Table: Summary of nonlinearities

region \forcing	ocean heat fluxes	land-sea contrast	topography
Northwest Pacific	isolated nonlinear response weaker	isolated nonlinear response weaker	linear
Western North America	ridge only in full nonlinear	ridge only in full nonlinear	ridge only in full nonlinear
Western Atlantic	linear	not important	isolated nonlinear response weaker
European sector	isolated nonlinear response weaker	isolated nonlinear response weaker	not important
Central Eurasia	not important	not important	isolated nonlinear response stronger

LIST OF FIGURES

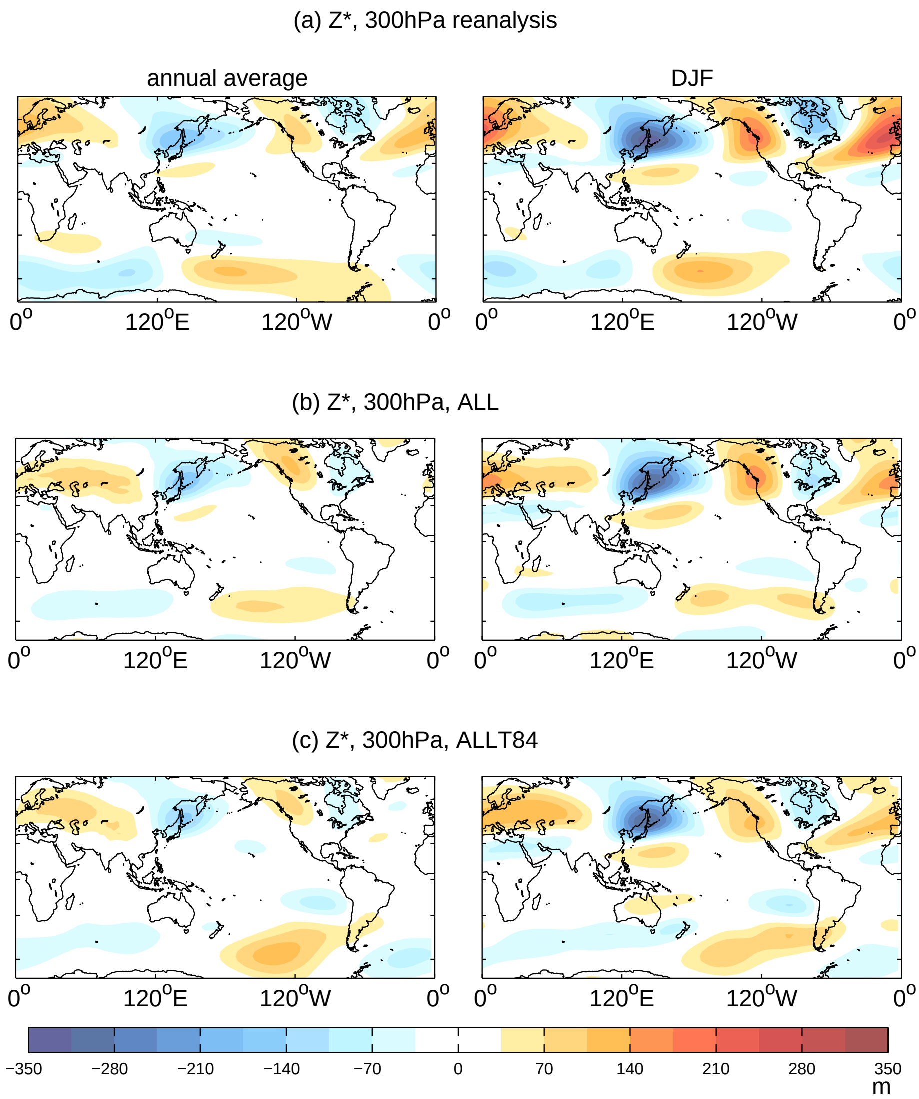

FIG. 1. Geopotential height at 300hPa in meters in the annual average and in December through February (a) in MERRA reanalysis, (b) in ALL, the most realistic integration (integration 7 on Table 1), (c) T84 ALL integration. The contour interval is 35m.

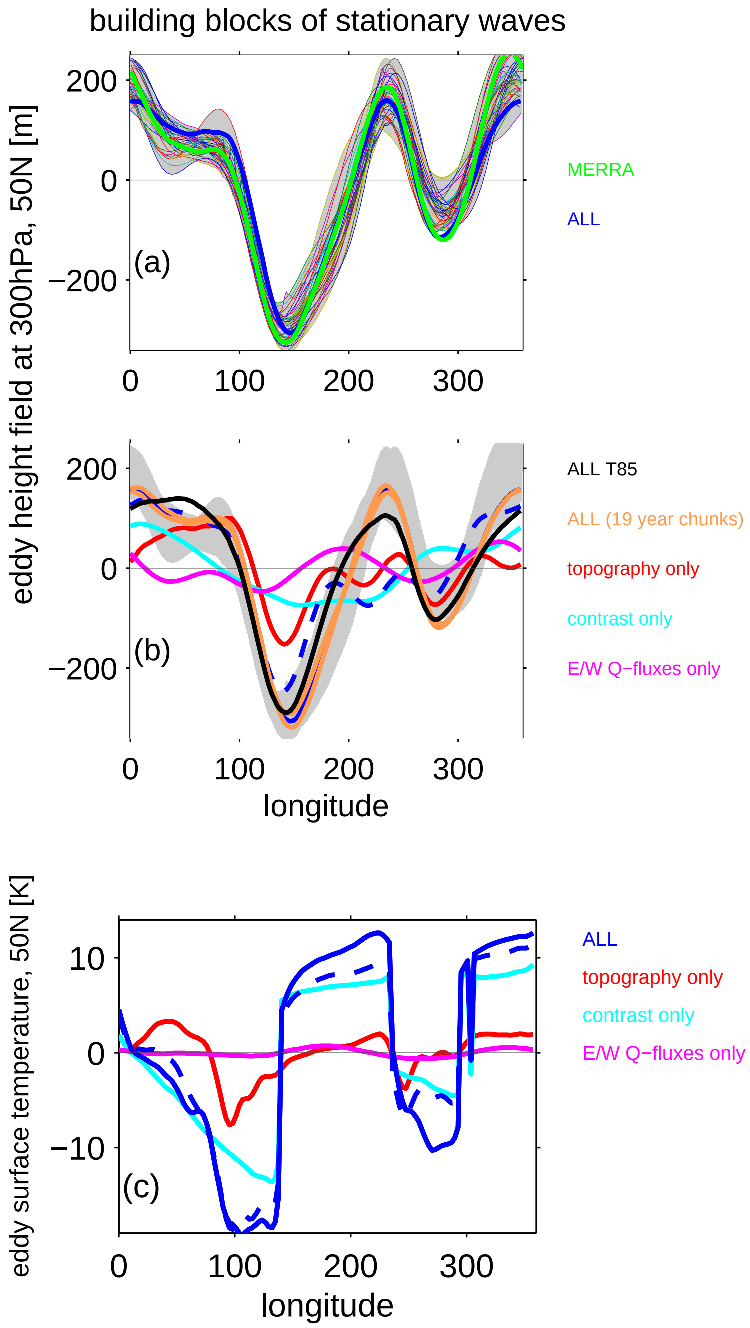

FIG. 2. Deviation of 300hPa geopotential height at 50N from the zonal average in (a) MERRA reanalysis (green), the most realistic MiMA integration in which all forcings are included (blue), 42 different CMIP5 models (thin lines), and the maximum and minimum for the 42 CMIP5 models (gray). (b) as in (a) but for the first 19 and second 19 years of ALL (orange), ALL performed at T84 resolution (black), integrations with topography only, land-sea contrast only, and ocean heat fluxes only (red, cyan, and magenta), and for the sum of these three integrations (dashed blue). The stationary waves in MiMA are compared to those present from 2009 to 2029 in the RCP8.5 integrations from 42 CMIP5 models. (c) is as in (b) but for surface temperature at 50N.

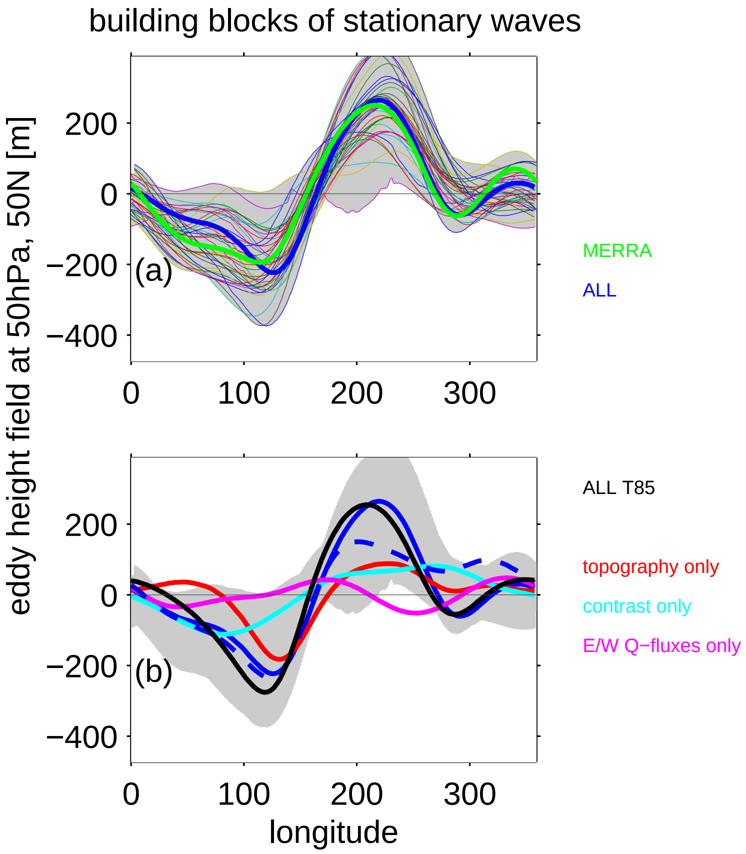

FIG. 3. As in Figure 2 but for 50hPa.

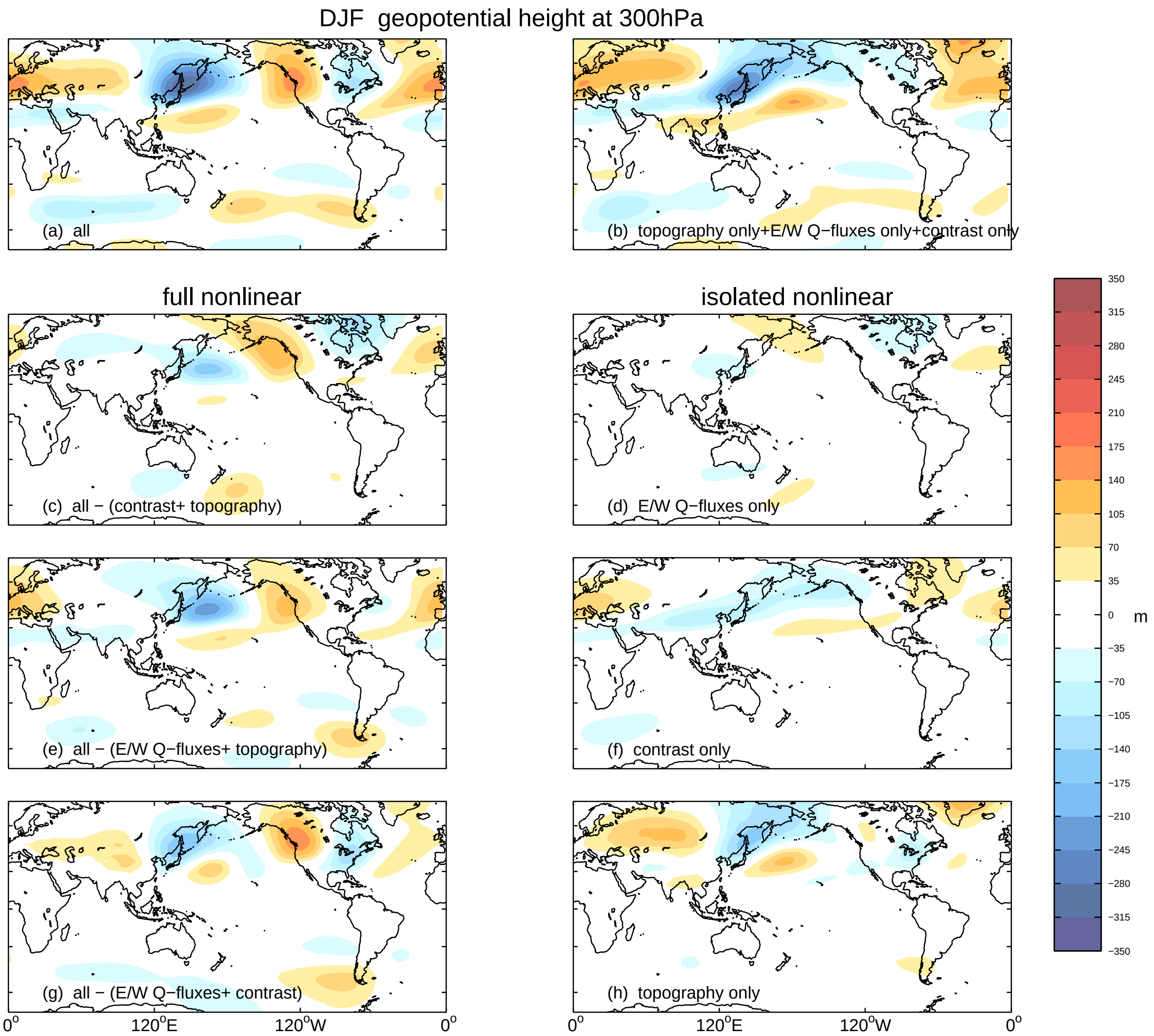

FIG. 4. Deviation of December through February 300hPa geopotential height from the zonal average in ALL (blue), (b) as in (a) but for the sum of integrations with topography only, land-sea contrast only, and ocean heat fluxes only; (c) the difference between ALL and the integration with land-sea contrast and topography; (d) integration with only ocean heat fluxes, (e) the difference between ALL and the integration with ocean heat fluxes and topography; (f) integration with only land-sea contrast; (g) the difference between ALL and the integration with ocean heat fluxes and land-sea contrast; (h) integration with only topography. The contour interval is 35m.

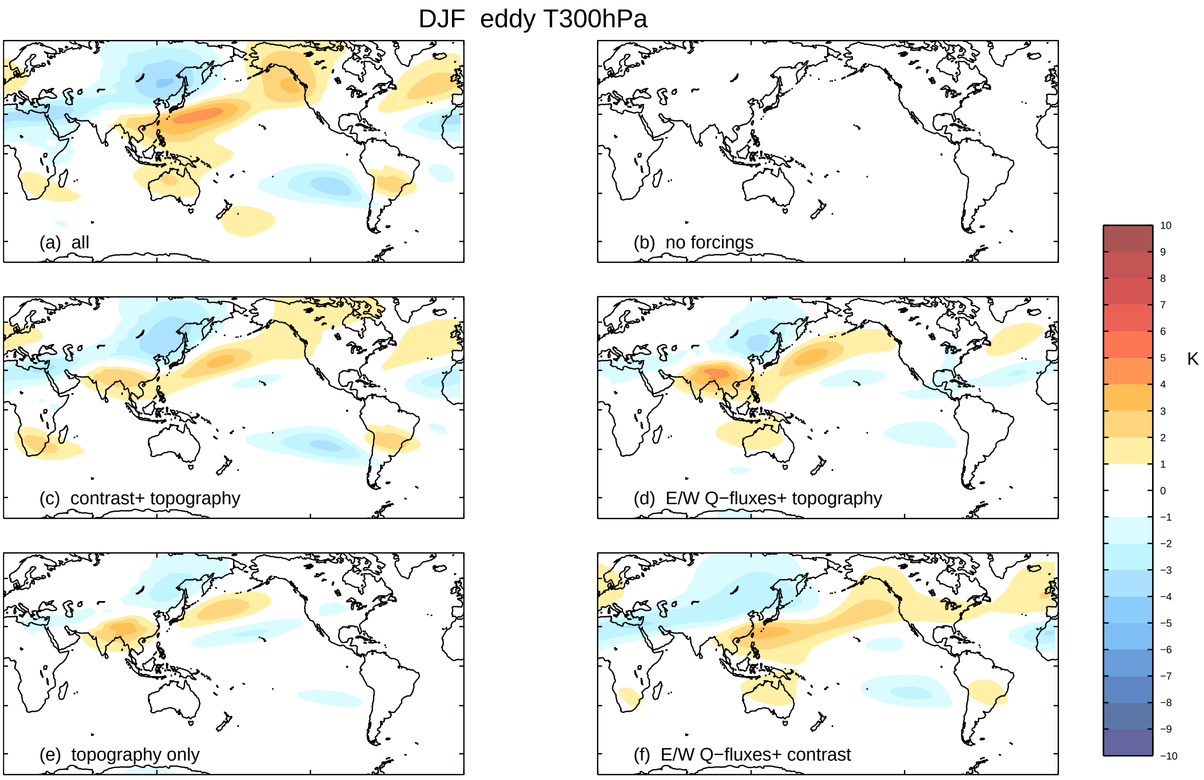

FIG. 5. The zonally asymmetric component of the 300hPa temperature field that is acted upon by the various forcings in (a) ALL, (b) a configuration with no zonally asymmetric forcings, (c) an integration with both land-sea contrast and topography, (d) an integration with both ocean heat fluxes and topography, (e) an integration with topography only, and (f) an integration with both land-sea contrast and ocean heat fluxes.

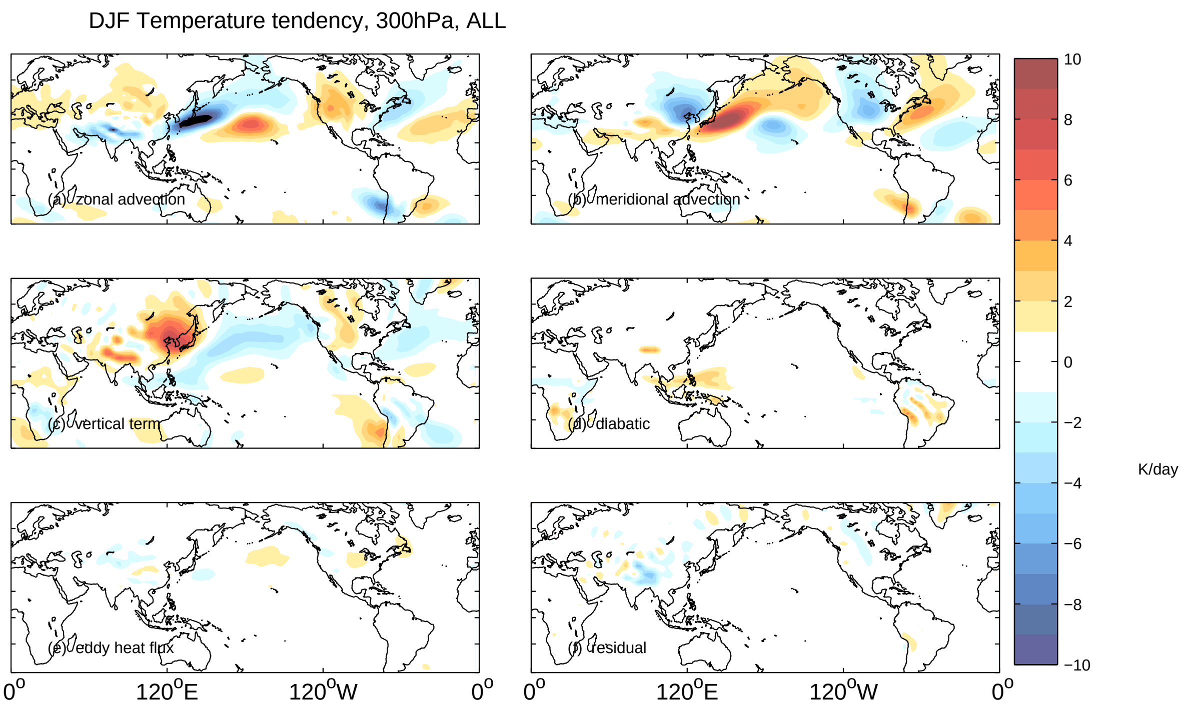

823 FIG. 6. Zonally asymmetric steady state thermodynamic balance for ALL following Wills and Schneider
824 (2018). (a) zonal advection term; (b) meridional advection term; (c) vertical term; (d) diabatic heating term; (e)
825 transient eddy heat flux term; (f) residual of the budget. The contour interval is 1K/day.

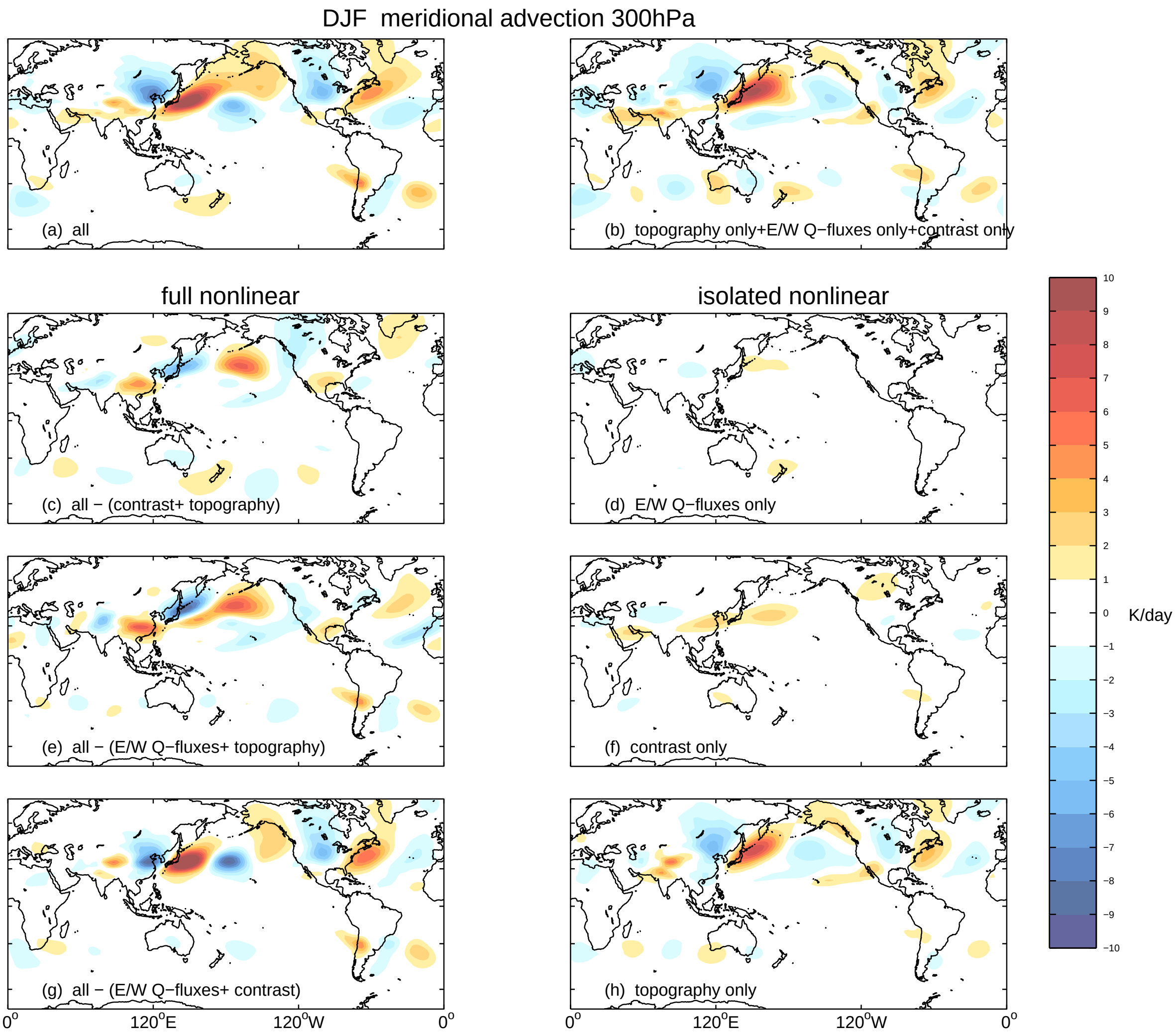

826 FIG. 7. As in Figure 4 but for the meridional advection term of the thermodynamic budget. The contour

827 interval is 1K/day.

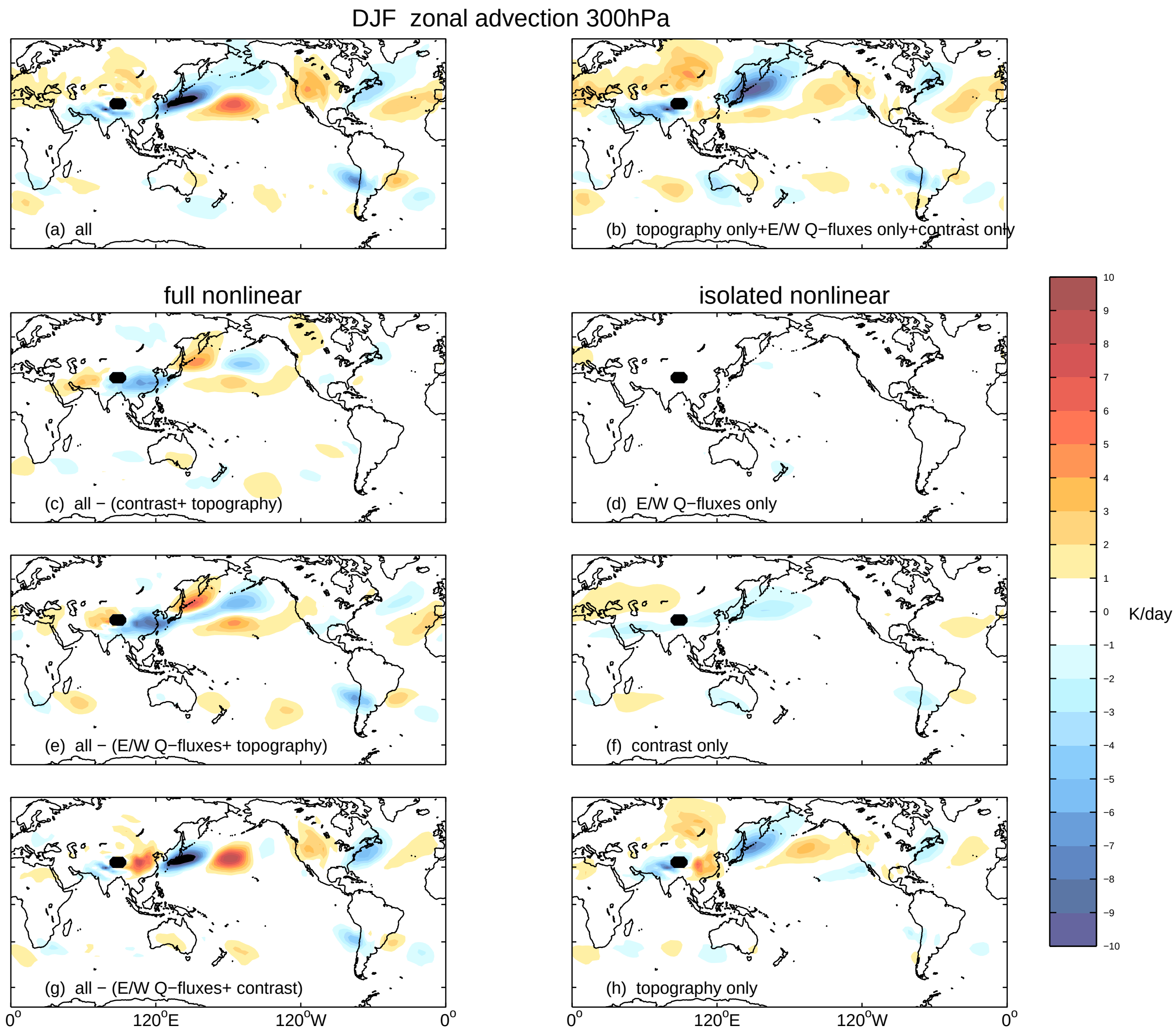

828 FIG. 8. As in Figure 4 but for the zonal advection term of the thermodynamic budget. The contour interval is
829 1K/day.

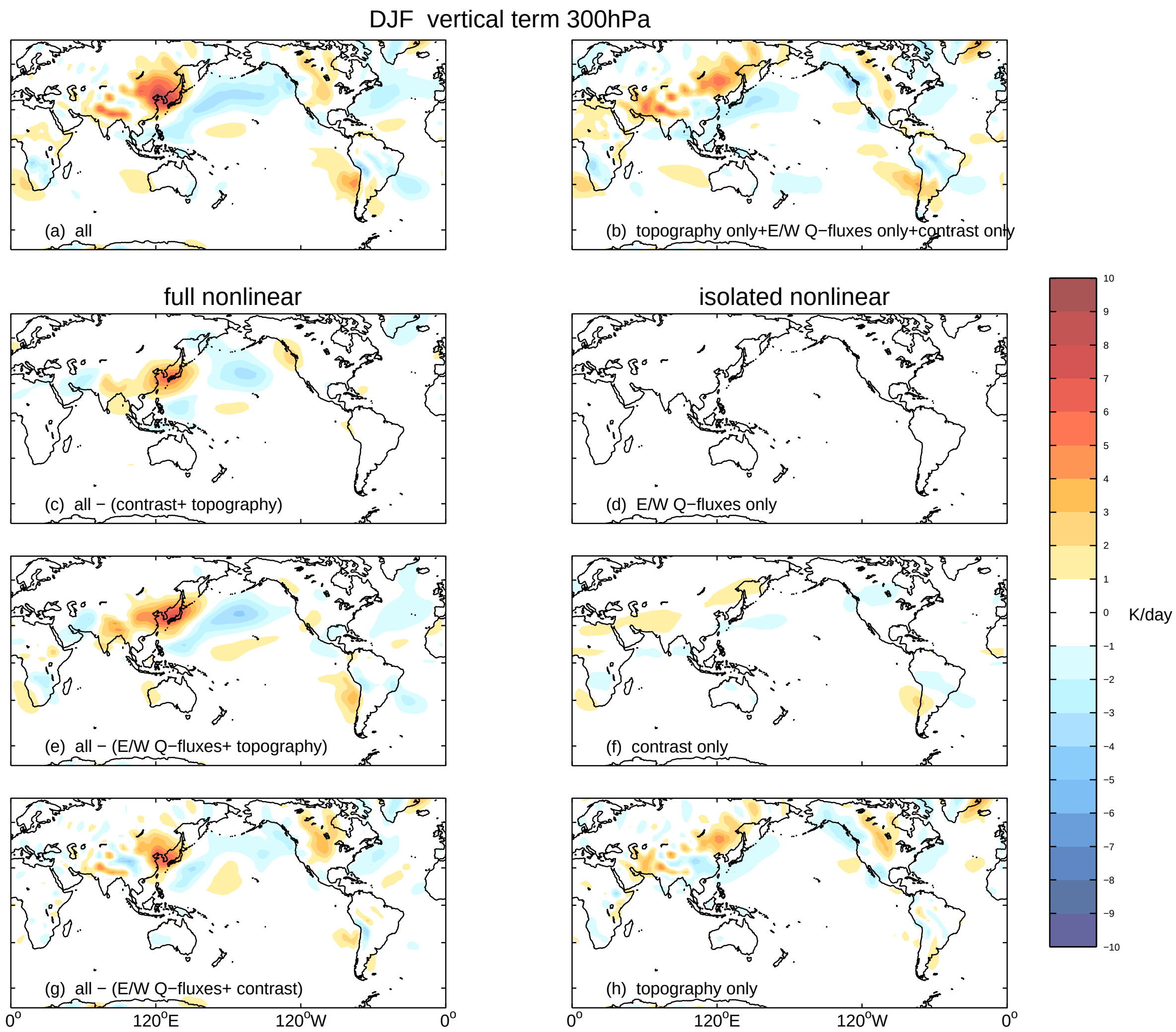

FIG. 9. As in Figure 4 but for the vertical term of the thermodynamic budget. The contour interval is 1K/day.

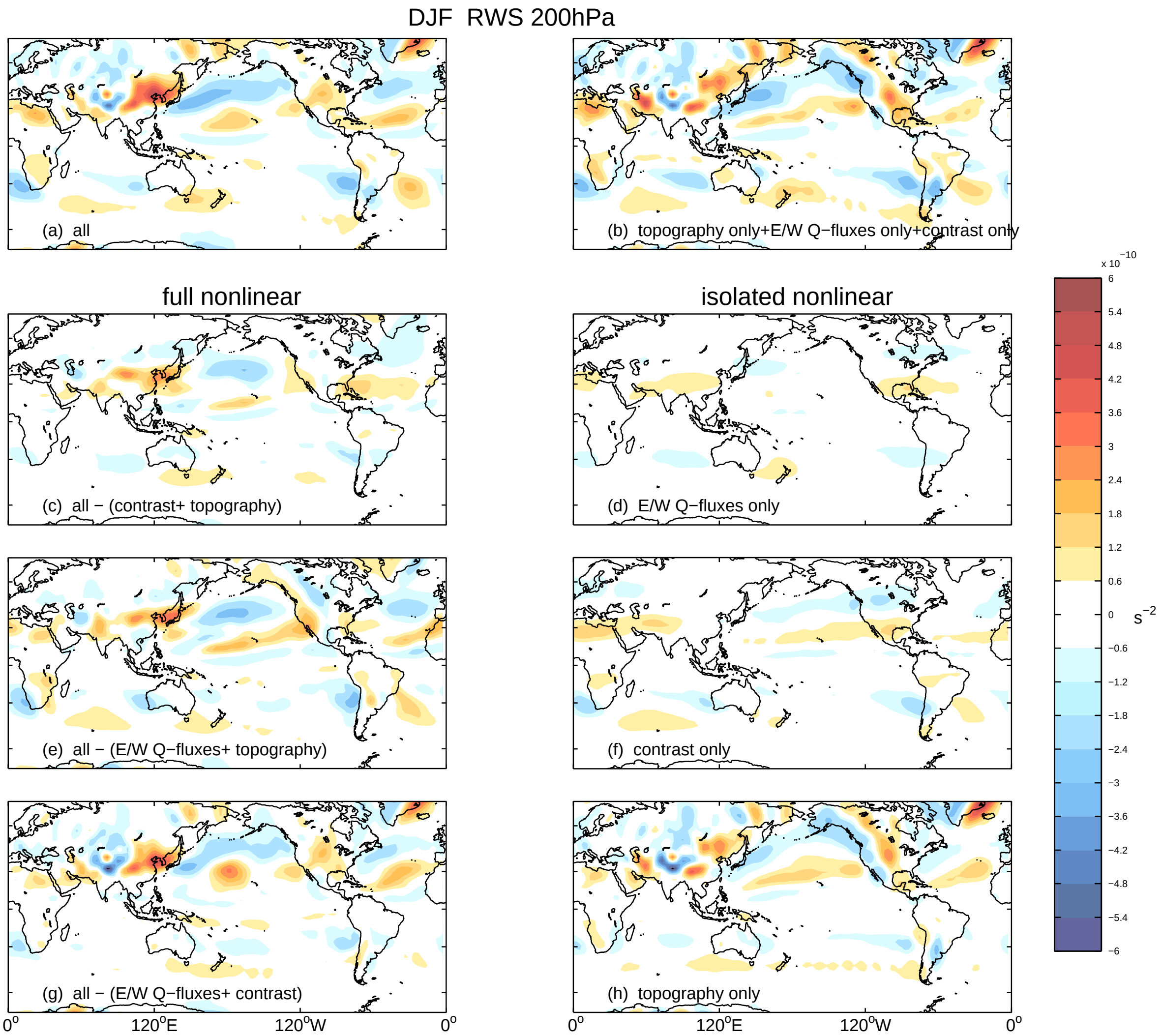

FIG. 10. As in Figure 4 but for the Rossby wave source calculated as in Sardeshmukh and Hoskins (1988). The contour interval is $6\times10^{-11}s^{-2}$.

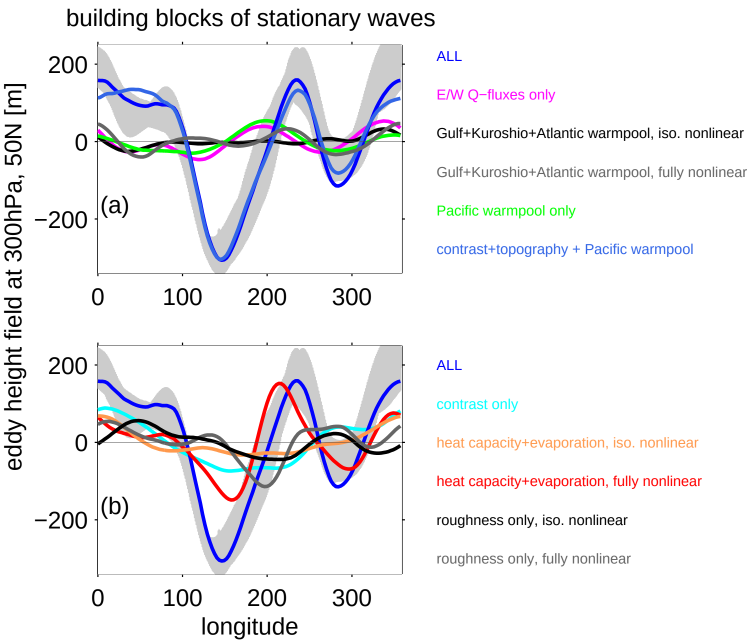

FIG. 11. As in Figure 2 but exploring the nonlinearities in the response to (top) ocean heat fluxes and (bottom) land-sea contrast. The isolated nonlinear and full nonlinear responses are defined in the text.